NASA TM X-62,018

NASA TECHNICAL MEMORANDUM

NASA TM X-62,018

IN-SITU MEASUREMENT OF OBJECTIVE LENS DATA OF A HIGH-RESOLUTION ELECTRON MICROSCOPE

Klaus Heinemann

Ames Research Center
Moffett Field, Calif. 94035

February 1971

In-Situ Measurement of Objective Lens Data of a High-Resolution Electron Microscope

By Klaus Heinemann

Ames Research Center, NASA

Moffett Field, Calif. 94035

Abstract

Bragg-reflex images of small individual crystallites in the size range of 20 - 100Å diameter with known crystallographic orientation were used in a transmission electron microscope to determine in-situ: (a) the relationship between objective lens current (or accelerating voltage) changes in discrete steps and corresponding defocus, (b) the spherical aberration coefficient, and (c) the axial chromatic aberration coefficient of the objective lens. The accuracy of the described method is better than 5%. The same specimen can advantageously be used to properly aline the illuminating beam with respect to the optical axis.

Zusammenfassung

Unter Verwendung von Bragg-Reflex-Bildern kleiner isolierter Kristallite in der Größenordnung von 20 - 100 Å im Durchmesser mit bekannter kristallographischer Orientierung konnten in situ (a) die Beziehung zwischen Feinregelstufen des Objektivstromeinstellers (oder des Beschleunigungsspannungseinstellers bei Mikroskopen mit Hochspannungs-Fokussierung) und resultierender

Defokussierungsdifferenz, (b) der Öffnungsfehlerkoeffizient 3. Ordnung und (c) der axiale Farbfehlerkoeffizient der Objektivlinse eines Durchstrahlungs-Elektronenmikroskops bestimmt werden. Die Genauigkeit der beschriebenen Methode ist besser als 5%. Es wird theoretisch begründet und experimentell bestätigt, daβ dasselbe Objekt vorteilhaft zur Feinzentrierung des Beleuchtungsstrahles verwendet werden kann.

1. Introduction

Knowledge of basic objective lens data and control over the electron beam alinement are often desirable - if not imperative - in high resolution electron microscopy.

In this paper we will outline the theoretical basis and describe the experimental application of a relatively simple method of determining the dependence of the defocus $\delta z(\Delta I)$ on the objective lens current. Then the spherical and chromatic aberration coefficients, C_3 and C_F, respectively, can be measured and a final microscope alinement which is sufficient for high resolution microscopy can be accomplished.

This work became particularly necessary when the objective lens current of our Siemens Elmiskop 101 was increased with the intention of reducing the existing aberration coefficients.

The usual approach to determine $\delta z(\Delta I)$ is based upon the defocus dependent phase contrast transfer characteristics of the objective lens in the normal mode

of operation [1] which is characterized by three-wave interference. A high-quality defocus series of any specimen containing a continuous spectrum of space frequencies, preferably a thin carbon foil, has to be furnished and examined in a light optical diffraction device [2]. Such a Fourier analysis of reciprocal space frequencies usually results in a set of concentric rings with varying width and diameter. For the final computation of $\delta z\,(\Delta I)$ these patterns must be evaluated, preferably graphically with the use of phase contrast transfer characteristics (see fig. 2 in [1]).

A prerequisite for this method is knowledge of the spherical aberration coefficient C_3 which is usually calculated from the magnetic field distribution along the optical axis (see [3] p. 373 and [4]) and often supplied by the manufacturer of the microscope. However, the value of C_3 applies to a specific operation of the lens and significantly depends on such parameters as vertical specimen position, objective lens current, and pole piece geometry. If these parameters are changed, the factory-supplied value of C_3 is no longer applicable, and a new calculation or measurement of C_3 is required in order to apply the common method of determining $\delta z\,(\Delta I)$ (a relatively accurate but rather complicated method).

Another common method of determining $\delta z\,(\Delta I)$ is to change the focal length of the objective lens using washers of a known thickness b and to measure the lens current I required for each vertical specimen position. The relationship between δz and ΔI can then be calculated as the slope of b vs. I.

A much easier and equally accurate way of determining $\delta z(\Delta I)$ is described here. This method does not require knowledge of the spherical aberration coefficient. Furthermore, the spherical and chromatic aberration coefficients can be determined in-situ almost simultaneously and the microscope alinement can be controlled.

2. Bragg Reflex Images

Often when crystalline material is observed in an electron microscope, bright reflex images are noticeable and move over the screen upon defocusing. They are due to Bragg scattering at crystal lattice planes parallel to the incident electron beam. These images have been used to determine the orientation of evaporated thin island films [5]. Hall [6] used them in an experimental determination of C_3 similar to our approach described later on.

This present paper is based upon observations made on such crystalline material. For specimens we used thin films of gold nucleated on mica. The thin deposits consisted of particles of about 50 Å average diameter and a number density of several 10^{10} particles per cm^2. The particles were usually {111}- or {211}-oriented, and some were multiply twinned. Thus, {220}- and {111}-reflex images of gold could be observed frequently.

3. Measurement of $\delta z(\Delta I)$

In the following considerations we will identify the electron optical axis with the z-axis of an x, y, z-Cartesian coordinate system. We select a representation in complex units ($u = x + iy$) for locations in the x, y-plane in order to facilitate the incorporation of lens astigmatism in this formation. Electrons originating from a point $u_o = 0$ in the specimen plane $z = z_o$ will then intersect the image plane $z = z_1 + M^2 \Delta z_o$ at a distance

$$u = u(z_1 + M^2 \Delta z_o) = M(C_3 u_o'^2 \bar{u}_o' - \Delta z_o u_o' - C_a \bar{u}_o') \tag{1}$$

from the optical axis (see [7] eq. (5.27) and [8], eq. (5) for $u_o = 0$), if the paraxial approximation is employed. Indices 0 and 1 represent values in specimen and gaussian image plane, respectively. Since in electron optics defocus values are usually referred to distances in the specimen plane, we will use the expression $\Delta z_1 = M^2 \Delta z_o$ as defocus from the gaussian image plane; M is the magnification; $\bar{u} = x - iy$ is the conjugate complex value of u; C_a is half the astigmatic defocus difference; primes represent derivatives with respect to z. Thus, the magnitude of u_o' and $\bar{u}_o'$, respectively, represents the objective aperture $\alpha_o = 2\vartheta_B$. We form

$$\delta u = u(z_1 + M^2 \Delta z_o^{(2)}) - u(z_1 + M^2 \Delta z_o^{(1)})$$

$$= M(\Delta z_o^{(1)} - \Delta z_o^{(2)}) u_o' = M u_o' \delta z_o \tag{2}$$

This equation can be verified experimentally and used easily for measuring the defocus dependence on the object lens current. One simply has to measure the shift on the final microscope screen, δr, of the reflex images per unit step of the objective lens current change, ΔI, and to insert this value as magnitude of the complex unit δu in equation (2). Then $\delta z(\Delta I)$ is given by

$$\delta z(\Delta I) = \frac{\delta r(\Delta I)}{2M\vartheta_B} = \frac{d}{M\lambda}\,\delta r(\Delta I) \qquad (3)$$

In (3), d represents the lattice plane separation corresponding to the Bragg angle ϑ_B by use of the Bragg equation $d = \lambda/2\vartheta_B$.

An example is shown in Fig. 1. Between the micrographs a) and b) the objective lens current was changed by 56 fine steps of the lens current control (equivalent to $\Delta I/I = 6.97 \cdot 10^{-4}$). The shift of the Au-{111}-reflex images (see schematic summary c) amounts to $\delta r/M = 230$ Å related to distances in the specimen plane. If we insert this in equation (3), a value of $\delta z = 26$ nm per fine step of the lens current control results.

The accuracy of this method depends mainly upon the tolerance with which the magnification can be specified. We calibrated the magnification of our microscope (Siemens Elmiskop 101) with the help of images of {111}-lattice planes of gold with 2.353 Å separation. Since we were able to image more than 50 {111}-lattice planes (see Fig. 2), an accuracy in magnification calibration of better than 1% could be obtained easily.

The accuracy of this $\delta z(\Delta I)$ - determination is also affected by the precision within which the movement of the reflex images can be determined. It is not better than about 5% for the evaluation of bright field images, mainly because of the defocus-dependent phase contrast transfer characteristic of the objective lens in this mode of operation, which gives rise to a rather uneven background at larger defocuses.

The accuracy can be increased significantly when central dark field imaging methods are applied (see Fig. 1 d-h) We used a 6 micron wire centered across the opening of a disk aperture as beam stop, thus allowing only those electrons to pass that had been scattered at the specimen. The diameter of the aperture was large enough to allow $\{111\}$- and $\{220\}$- Bragg scattered electrons to pass. In this mode of two-beam-interference operation we do not have any dependence of the background phase contrast upon the amount of defocus, as Hanszen and Morgenstern [10] postulated theoretically and Thon [11] has shown experimentally. The reflex images appear with high contrast on a significantly darker background. Shifts of the reflex images of the order of 200 nm (60 mm on the microscope screen at M = 300,000) could be detected easily and measured with an accuracy of about 2%. In both bright field and central dark field microscopy, we could improve the measuring accuracy by taking advantage of the fact that, in general, two reflex images exist which shift symmetrically with respect to the steady bright field image (naturally missing in the case of central dark field

operation) upon defocusing. For clarity, however, only one of the two reflex images of each crystallite, the ones indicated by an arrow in Fig. 1, have been used for the schematic summaries in c and i of this figure.

We found that it is often convenient to have a microscope screen with a calibrated coordinate system (in polar coordinates). With the help of such a scale micrographs are unnecessary for the measurement of the shift of the reflex images.

The final result of the δz determinations, applicable for our normal objective lens of the Siemens Elmiskop 101, operated at 100 kV accelerating voltage and at increased lens current of 580 mA, was $\delta z = 26.3$ nm $\pm 2\%$ per fine step of the lens current control.

4. Determination of the Spherical Aberration Coefficient

Due to spherical aberration, Bragg scattered electrons originating from a specimen point on the optical axis will intersect the optical axis prior to reaching the gaussian image plane. This occurs at a defocus of

$$\Delta z = 4 C_3 \vartheta_B^2 \tag{4}$$

This result can be obtained from equation (1) for $u'_o \bar{u}'_o = |u'_o|^2 = \alpha_o^2 = 4\vartheta_B^2$ and negligible astigmatism.

We used this relationship for an in-situ determination of C_3 and found that it was possible to measure this lens constant within an accuracy of 5%. The

most accurate previously reported measurement of the spherical aberration coefficient was that of Kunath and Riecke [12] who superimposed two images of the same specimen area, one taken at axial and one at tilted illumination, and measured the resulting shift $MC_3\alpha_o^3$ of a characteristic specimen point. The calibration of the tilting angle was performed by the use of a T1C1 specimen in selected area diffraction. The accuracy of this method was about 10%. Hall [6], as mentioned earlier, used the reflex images for determining C_3. Instead of directly measuring Δz, however, he measured the characteristic shift δr of the reflex images at the gaussian focus and was therefore, in principle, not able to perform in-situ measurements. His accuracy was less than 10%. The procedure of the C_3-determination used here is very simple. The pairs of reflex images on the microscope screen are visually superimposed over the bright field image (formed by axial, nonscattered electrons) at a sufficiently high magnification (about 200,000 ×). Then we refocus until the minimum of background detail phase contrast has been reached. This indicates in good approximation the gaussian image plane. The total amount of defocus difference Δz which has to be known for computation of C_3 according to equation (4) is the number of fine steps of the objective lens control necessary for this refocus multiplied by the calibrated amount of defocus difference per single control step.

For more exact determination of C_3 one has to consider that the mentioned contrast minimum does not occur exactly in the gaussian image plane (see, for example, [2] Abb. 1 and 2) but at a small underfocus, which itself is dependent on C_3, as the following consideration proves. The phase contrast transfer characteristic can be represented graphically as an array of curves in a coordinate system with defocus Δz and objective aperture α_o as Cartesian coordinates, computed from the equation

$$\Delta z = (2n - 1)\frac{\lambda}{2\alpha_o^2} - \frac{\alpha_o^2 C_3}{2} \tag{5}$$

for $n = 0, \pm 1, \pm 2, \ldots$ [1]. These curves, indicating conditions for maximum phase contrast, are shifted toward the underfocus direction, due to the second term in (5), when compared with equivalent curves for the ideal lens, characterized by $C_3 = 0$. This shift is a function of α_o and amounts to

$$\Delta z_s = \frac{\alpha_o^2 C_3}{2} \tag{6}$$

Most likely, the contrast minimum will occur near that defocus which lies midway between the phase contrast transfer functions with $n = 0$ and $n = 1$ for $\alpha_o = \alpha_{oa}$ corresponding to the apex of the transfer function with $n = 0$. We obtain the apex coordinates by forming

$$\frac{d[\Delta z(n = 0)]}{d\alpha_o} = \frac{\lambda}{\alpha_o^3} - \alpha_o C_3$$

and find

$$\alpha_{oa} = \left(\frac{\lambda}{C_3}\right)^{\frac{1}{4}} \tag{7}$$

We insert (7) for α_o in (6) and obtain

$$\Delta z_{CM} = -\frac{1}{2}(\lambda C_3)^{\frac{1}{2}} \tag{8}$$

as defocus at the contrast minimum. For $C_3 = 3.2$ mm and $\lambda(100\,\text{kV}) = 3.7 \cdot 10^{-3}$ nm we get $\Delta z_{CM} \approx -55$ nm. The experimental evidence of this behavior is given in Fig. 3. The specimen, an amorphous carbon film, was tilted 22° with respect to the image plane. Consequently, a monotonically changing defocus occurred along the specimen direction which was normal to the tilting axis. The calibration of the scale indicating the local amount of defocus was done with a light optical diffractometer. One clearly recognizes the contrast minimum at an underfocus between about 40 and 60 nm. This difference in Δz between the gaussian focus and the contrast minimum is relatively small compared to the total defocus necessary for superimposing the reflex images, approximately 750 and 2000 nm for {111}- and {220}-reflex images of gold, respectively.

The accuracy of the described method of determining C_3 is also affected by the illumination aperture α_b since the effective objective aperture angle for a Bragg-scattered electron is not exactly ϑ_B but falls within the limits $2\vartheta_B - \alpha_b$ and $2\vartheta_B + \alpha_b$. This error can be eliminated experimentally to a certain extent if we evaluate only pairs of reflex images which appear with the same intensity

on the microscope screen, indicating an optimum parallel alinement of the crystal lattice planes with respect to the optical axis. Furthermore, a small illumination aperture itself and higher order reflex images, such as {220}- rather than {111}- reflex images of gold, are advantageous for an accurate determination of C_3.

When all these precautions are taken into consideration, the result for our microscope lens, again operated at 580 mA lens current, was $C_3 = 2.25\,\text{mm} \pm 3\%$.*

5. Determination of the Axial Chromatic Aberration Coefficient

Relative variations in accelerating voltage U^* (with relativistic correction) and in the objective lens magnetic field B can be expressed in terms of a defocus difference δz

$$\delta z = \left(\frac{\Delta U}{U^*} + 2 \frac{\Delta B}{B} \right) C_F \qquad (9)$$

see [13]. If the objective lens is not operated in magnetic saturation we have the simple relationship $\Delta B/B = \Delta I/I$ between relative variations in magnetic field

---

*Once the spherical aberration coefficient has been determined, this method can be used advantageously for determining in-situ the orientation of isolated small crystallites. The Bragg-angle ϑ_B, to which the observed reflex images belong, can then be easily determined by eq. (4). The azimuthal orientation of the crystal is given by the direction of shifting of the reflex images (see [5]).

and objective lens current. This is the case for the Siemens Elmiskop 101 objective lens under standard operating conditions to a good approximation. Therefore, a determination of C_F according to

$$C_F = \frac{\delta z_o}{2(\Delta I/I)} \tag{10}$$

is possible with the results of the $\delta z(\Delta I)$ determination (defocus difference per unit step of the lens current control) previously described. We obtained $\delta z_o = 65$ nm per $\Delta I/I = 1.56\ 10^{-5}$ and thus $C_F = 2.1$ mm which complies with the factory-supplied value of C_F under standard conditions.

If the objective lens is partly operated in saturation (i.e., if $\Delta I/I > \Delta B/B$), an exact determination of C_F can be made only if discrete changes are made to the accelerating voltage instead of the lens current. However, a calculation using lens current changes can still be useful, as the result reveals the effective chromatic sensitivity with respect to lens current changes. Thus, for example, the increase of the total lens current to 580 mA, resulting in $\delta z_o = 26.3$ nm per $\Delta I/I = 1.24\ 10^{-5}$, decreased the value of the effective chromatic aberration coefficient, as applicable to current variations only, by a factor of 2.

6. Test and Performance of Final Microscope Alinement

According to Haine [14] and Riecke [15] a good microscope alinement should be achievable under the following conditions:

(a) The image point which does not change its location upon reversing the lens current polarity ("polarity center") has to be centered on the final microscope screen by shifting the projective lens.

(b) The image point which does not change its location upon defocusing ("current center" or "voltage center" referring to changes of lens current or accelerating voltage as usual means for defocusing the image) has to be centered on the screen by properly adjusting the direction of the illuminating beam.

In connection with an extensive, usually factory-performed, prealinement of the microscope that provided for minimum deviations from rotational symmetry within the objective lens and a proper alinement of the intermediate lens with respect to the optical axis determined by objective and projective lenses, this procedure was usually sufficient as long as the microscope was operated under normal conditions. When, however, the current of the standard Siemens Elmiskop 101 objective lens was increased from 480 mA to 580 mA, the current center alinement was no longer satisfactory. This is probably due mainly to magnetic stray fields affecting the rotational symmetry along the optical axis which is caused by saturation in the magnetic circuit of the objective lens. Kanaya and Ishikawa [16] earlier proposed to apply a voltage center alinement rather than a current center alinement. Experiments showed that there exists a considerable difference between voltage and current centers in our case of higher lens current, whereas this difference was negligible at normal operating conditions, and that,

indeed, a voltage center alinement represented a better approach than the current center alinement. (The lens itself had been mechanically prealined to the extent that the difference between the current centers in both polarities was less than 3 μm, as referred to distances in the specimen plane.)

Leisegang [17] reports an alinement method which is characterized by centering that area of a low-magnification image of specimen containing many small holes which shows concentric interference phenomena around and within the holes. We tested this method and found it quite useful, although it is not as accurate as the "reflex image alinement" method described here.

Starting point for the final alinement was a pre-alinement which provided for a minimum distance between the current centers in both lens current polarities. We shall consider the defocus dependence of both the positive and negative first-order reflex images and the zero-order bright field image, and use the indices +1, -1, and 0, respectively. $v' = |v'|e^{i\varphi_0}$ is representative of tilting angle $|v'|$ and azimuthal direction φ_0 of the incident electron beam, $w' = |w'|e^{i\varphi_1}$ indicates the respective data of the Bragg-reflected part of the beam. Equation (1) turns then into the following expressions for the three cases to be discussed.

$$u_{\pm 1} = M[(C_3|v' \pm w'|^2 - \Delta z)(v' \pm w') - Ca(\bar{v}' \pm \bar{w}')]$$

$$u_o = M[(C_3|v'|^2 - \Delta z)v' - Ca\bar{v}'] \qquad (11)$$

For these equations the relationship $u'\bar{u}' = |u'|^2$ was used.

We discuss at first the behavior for $v' = 0$ (i.e., for alined illumination). In this case (11) becomes

$$u_{+1} = M[(C_3|w'|^2 - \Delta z)w' - Ca\,\bar{w}'$$

$$u_o = 0$$

$$u_{-1} = M[(-C_3|w'|^2 + \Delta z)w' + Ca\,\bar{w}' \qquad (12)$$

and we find that all possible positions u_{+1} of the one reflex image with Δz as parameter are on a straight line within the complex coordinate system (representing the microscope image plane), as indicated by the dashed line in Fig. 4. Points A_{+1} and B_{+1} on this line indicate the special cases $\Delta z = 0$ and $\Delta z = C_3|w'|^2$; the arrow indicates the direction of movement of the reflex images upon increasing under-defocus. The dotted line displays the analog behavior for u_{-1}. A superposition of both reflex images can only be performed if the astigmatism has been corrected completely ($Ca = 0$). In this case the dotted and dashed lines coincide, and at a defocus of $C_3|w'|^2$ a superposition of B_{+1} and B_{-1} at the origin of the coordinate system - the geometrical location of u_o - takes place.

We consider now the case $v' \neq 0$. For reasons of clearness we assume $|v'| << |w'|$ and $C_a = 0$. This simplification can be justified because an incorrect alinement of the illuminating beam usually means that the illumination tilting

angle with respect to the electron optical axis of the microscope objective lens is at least one order of magnitude smaller than the Bragg angles used here, and the astigmatism can always be corrected sufficiently if $|v'| << |w'|$. Thus, we consider the behavior of the system of equations:

$$u_{\pm 1} = M(C_3|w'|^2 - \Delta z)(v' \pm w')$$

$$u_o = M(C_3|v'|^2 - \Delta z)v' \qquad (13)$$

In Fig. 5 the directions of v' and w' in the image plane are indicated by thick arrows. Again, all possible positions of u_{+1} and u_{-1} with Δz as parameter are indicated as dashed and jotted lines, respectively. Equation (13) and Fig. 5 give rise to the following conclusions:

- A superposition of both reflex images at the origin of the coordinate system (B_{+1}) can be obtained independently from illumination alinement.
- A total superposition of the two lines along which the reflex images move upon defocusing, (i.e., parallelism between both azimuthal directions of movement can generally not be obtained if $|v'| > 0$).
- If $|v'| > 0$ the zero-order bright field image also moves (slightly) over the screen upon defocusing. At $\Delta z = C_3|w'|^2$, the defocus required for superpositioning the two reflex images, this bright field image has a distance of

$$|u_o| \approx C_3 M|w'|^2|v'| \qquad (14)$$

(B_0 in Fig. 5) from the origin of the coordinate system, where the reflex images coincide.

- The distance of the two reflex images from the zero-order image (e.g., the distance of A_{+1} and A_{-1} from B_{+1}) is in general not equal.

This leads to three different criteria for a correct alinement of the illuminating beam. They are characterized by

1. Parallelism of the directions in which the reflex images move upon defocusing.
2. Superposition of the reflex images upon the bright field image (at the required defocus of $\Delta z = C_3|w'|^2$).
3. Symmetric location of the zero order image with respect to the two reflex images (preferably at $\Delta z \approx 0$).

Whereas it is experimentally rather difficult to take advantage of the first mentioned criterion - the angle between the two directions of movement is usually very small and can hardly be detected on the microscope screen - the other two criteria can advantageously be used for the experimental alinement procedure. Figure 6 illustrates the first of these two alternatives. The micrographs were taken at a defocus of 550 nm which provided for a superposition of the gold $\{111\}$-reflex images for $C_3 = 2.25$ mm and 100 kV accelerating voltage. In the cases (a) and (b) the illumination was intentionally tilted with respect to the optical axis (in two different 180° rotated azimuthal directions). The tilting

angles were $3.7 \cdot 10^{-3}$ and $2.3 \cdot 10^{-3}$ radian, respectively. A corresponding difference between the locations of bright field and superimposed reflex images can be noticed and measured to 20 Å (a) and 13 Å (b), if referred to distances in the specimen plane, which complies with eq. (14) (see schematic enlargements of outlined portion of the micrographs). The micrograph c of Fig. 6 was taken at alined illumination, which was obtained by observing the bright field and superimposed reflex images visually on the microscope screen and changing the tilting angle of the illuminating beam with the intention of reducing the distance between the observed bright field and reflex images. As can be seen, all images are now superimposed concentrically.

The alinement test according to criterion 3 (at $\Delta z \approx 0$) is demonstrated in Fig. 7 with the same specimen area used for Fig. 6. The micrographs of Figs. 7(a) and (b) were again taken at two different slightly tilted illumination settings. The outlined area 1 on the lower left hand side shows all three images on one straight line, which means that now points A_{-1}, B_o and A_{+1} in Fig. 5 lie on a straight line, indicating that the azimuthal directions of specimen illuminating beam and reflex images were approximately identical. Thus, an evaluation of the respective locations of reflex and bright field images can be used for an easy determination of the present illumination angle. As indicated, the zero-order image was measured to be 13 Å and 31 Å, respectively, off the center between the Au-{111}-reflex images. As this shift $|B_{+1}\, B_o|$ equals $C_3 |w'|^2 |v'|$, a

tilting angle of $|v'| = 2.3 \cdot 10^{-3}$ radian and $5.5 \cdot 10^{-3}$ radian, respectively, can be computed with eq. (14). Area 2 in Fig. 7 shows the behavior in the normal case where the azimuthal directions of v' and w' are different. It can be recognized clearly that the three images do not lie on a straight line in this case.

Figure 7c was taken at alined illumination ($|v'| \approx 0$), which was obtained by appropriately changing the illumination angle with the aim to maximize the degree of symmetry between the zero-order and reflex images visually on the microscope screen.

An alinement test at $\Delta z \approx 0$ avoids possible disadvantages caused by lack of depth of field which is quite common in the case of extreme defocus settings as required for superposition of higher order reflex images. For a final alinement at $\Delta z \approx 0$ it is generally necessary, however, to observe two particles showing reflex images in two different azimuthal directions, because the displacement of the reflex images with respect to the bright field image can easily be overlooked if the azimuthal directions of illuminating beam and reflex image movement are perpendicular, whereas the asymmetry is maximized in the case of parallel azimuthal directions (see Fig. 5 and schematic enlargement of particle 2 in Fig. 7a compared to particle 1 in the same print).

A beam could easily be alined within an accuracy of about $5 \cdot 10^{-4}$ radian with the described methods. The highest accuracy is in the lower 10^{-4} range,

corresponding to 5 Å misplacement of Au - {220} - reflex images. Figure 8 shows a micrograph of multiply twinned gold crystallites taken after an illumination alinement within about $5 \cdot 10^{-4}$ radian with respect to the optical axis. Lattice spacings of 2.35 Å were resolved in either direction, as well as lines with 1.7 and even 1.18 Å separation (the latter are half spacings of Au {111}). The micrograph, taken in the axial illumination mode, illustrates that the described alinement procedure meets the requirements for high resolution microscopy.

7. Conclusions

The relationship $\delta z(\Delta I)$ between lens current changes in discrete steps and corresponding defocus difference, a prerequisite for quantitative high-resolution electron microscopy, can be determined in-situ, without evaluating electron micrographs, by observation of the defocus dependent displacement of reflex images on the final microscope screen. Any specimen consisting of small (below 500 Å in diameter), well separated and randomly oriented crystallites with known lattice spacings can be used for this purpose. The defocus difference per fine step of the lens current control of a Siemens Elmiskop 101 with normal objective lens but increased lens excitation was measured within an accuracy of ±2% and found to be strongly reduced when compared to standard lens operation.

The same specimen was used for an in-situ determination of the spherical aberration coefficient C_3 with an accuracy of ±3%. It was found that the increase in objective lens current resulted in a considerable decrease in C_3.

The chromatic aberration coefficient C_F was also determined. An increase in the degree of magnetic saturation of the objective lens as a result of increasing the lens current gives rise to a drastic decrease of C_F. In this case, however, a distinction between current and high voltage variations is imperative.

The same test-specimens can finally be used for a proper in-situ alinement of the illuminating beam. Because of magnetic static stray fields due to the increase of objective lens current, the commonly used current center alinement method is no longer satisfactory. A new procedure is described that permits alinement of the illumination beam within an angle of about $1 \cdot 10^{-4}$ radian with respect to the optical axis. Experimental proof of the efficiency of this alinement method is given: A micrograph, taken in the axial illumination mode, showing periodic structures of 1.2 Å in gold crystallites in either azimuthal direction.

I would like to express my appreciation to Dr. H.R. Poppa for his encouragement, many interesting and helpful discussions, and help in critically revising the manuscript. This work was performed while holding a National Research Council Postdoctoral Associateship.

References

[1] F. Thon, Z. Naturf. 20a (1965), 1.

[2] F. Thon, Z. Naturf. 21a (1966) 476.

[3] W. Glaser, Grundlagen der Elektronenoptik, Springer-Verlag Wien, 1952.

[4] O. Jandeleit and F. Lenz, Optik 16 (1959) 87.

[5] H. Poppa, Kl. Heinemann and A. G. Elliot, to be published in J. Vac. Sci. Techn. 8, 2 (1971).

[6] C. E. Hall, J. Appl. Phys. 20 (1949) 631.

[7] P. A. Sturrock, Phil. Trans. Roy. Soc. A243 (1951) 387.

[8] F. Lenz, Optik 15 (1958) 393.

[9] Kl. Heinemann and H. Poppa, Appl. Phys. Ltrs., 16 (1970) 515.

[10] K. J. Hanszen and B. Morgenstern, Z. Angew. Phys. XIX, 3 (1965) 215.

[11] F. Thon, Proc. IVth Europ. Reg. Conf. Electr. Micr. Rome 1968, 127.

[12] W. Kunath and W. D. Riecke, Optik 23 (1965/66) 322.

[13] Yu. V. Vorobev and A. A. Vyazigin, Optics Spectr. 22 (1967) 261.

[14] M. E. Haine, J. Sci. Instr. 24 (1947) 61.

[15] W. D. Riecke, Optik 24 (1966/67) 397.

[16] K. Kanaya and A. Ishikawa, Bull. Electrotechn. Lab. 22 (1958) 641.

[17] S. Leisegang, Optik 11 (1954) 397.

FIGURE CAPTIONS

Fig. 1. Gold crystals on mica, showing {111}- and {220}-reflex images at different settings of the objective lens current control, (a,b) bright field and (d-h) central dark field. c and i are schematic summaries of a,b and d-h, respectively, for $\delta z(\Delta I)$-computation.

Fig. 2. Multiple twinned gold crystal with {111}-lattice planes of 2.353 Å separation, used for magnification calibration (conical illumination mode [9]).

Fig. 3. Amorphous carbon specimen with continuously changing defocus obtained by specimen tilting.

Fig. 4. Defocus-dependent location of reflex images (dashed and dotted lines) in the complex image plane in the case of correct specimen illumination but in the presence of axial astigmatism.

Fig. 5. Defocus-dependent location of reflex images (dashed and dotted lines) in the complex image plane in the case of corrected astigmatism but tilted specimen illumination.

Fig. 6. Micrographs and corresponding schematics of gold crystallites on carbon, with $\Delta z = 4 C_3 \vartheta_B^3$ (Au{111}) $\approx$ 550 nm under different illumination conditions (bright field image: solid circle, superimposed dark field images: dashed circle).

Fig. 7. Same specimen and under similar conditions as shown in Fig. 6, but with $\Delta z \approx 0$ (middle row: v′ and w′ coplanar; lower row: v′ and w′ not coplanar).

Fig. 8. Multiple twinned gold crystallites with {111}-lattice planes and half spacings resolved in different azimuthal directions (axial illumination, alinement within 5×10^{-4} radian to optical axis).

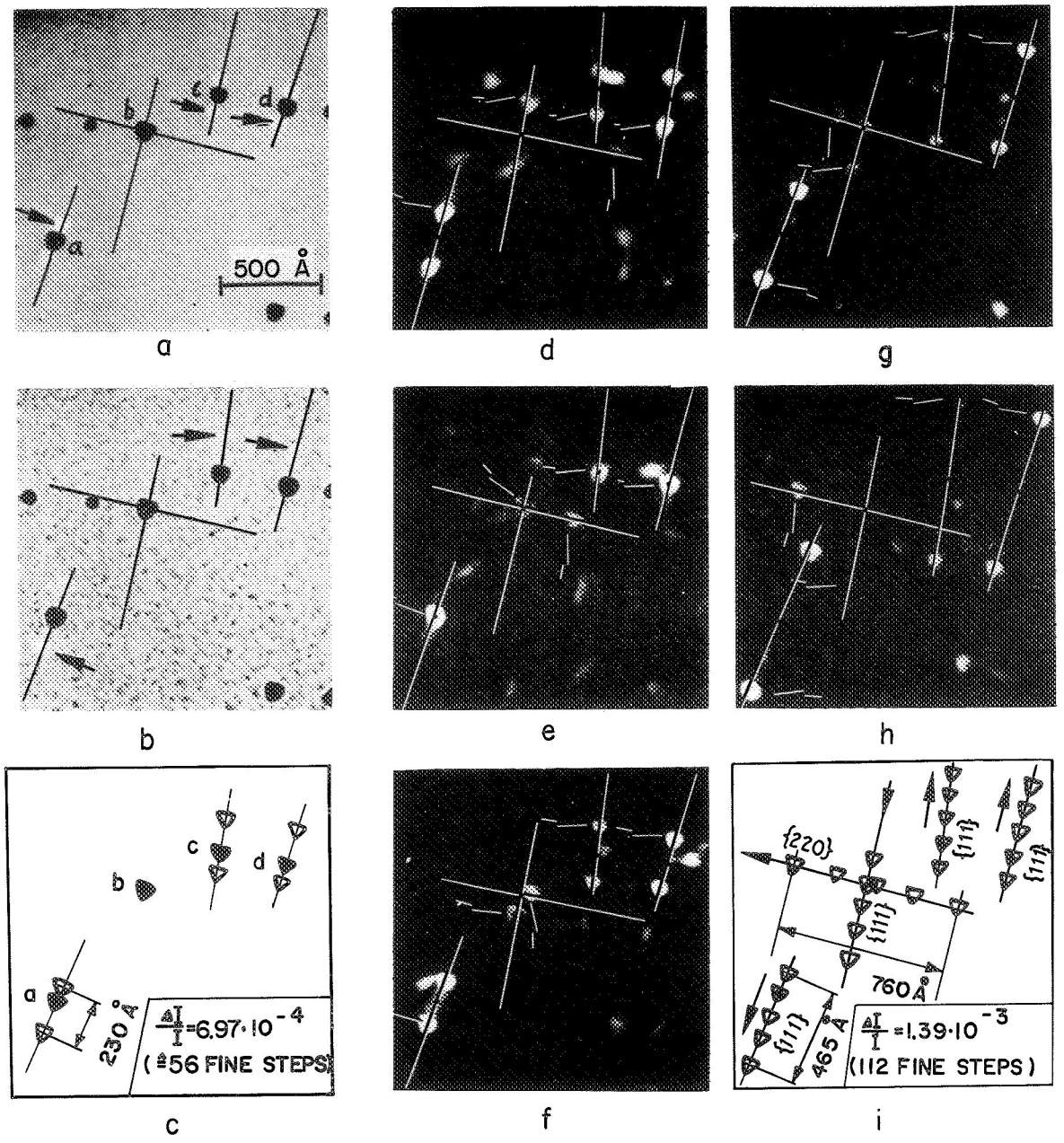
a
b
c
d
500 Å
a
d
g
b
e
h
b
c
d
a
230 Å
$\frac{\Delta I}{I}=6.97\cdot10^{-4}$
(≙56 FINE STEPS)
c
f
i
{220}
{111}
{111}
{111}
760 Å
465 Å
{111}
$\frac{\Delta I}{I}=1.39\cdot10^{-3}$
(112 FINE STEPS)

Figure 1.

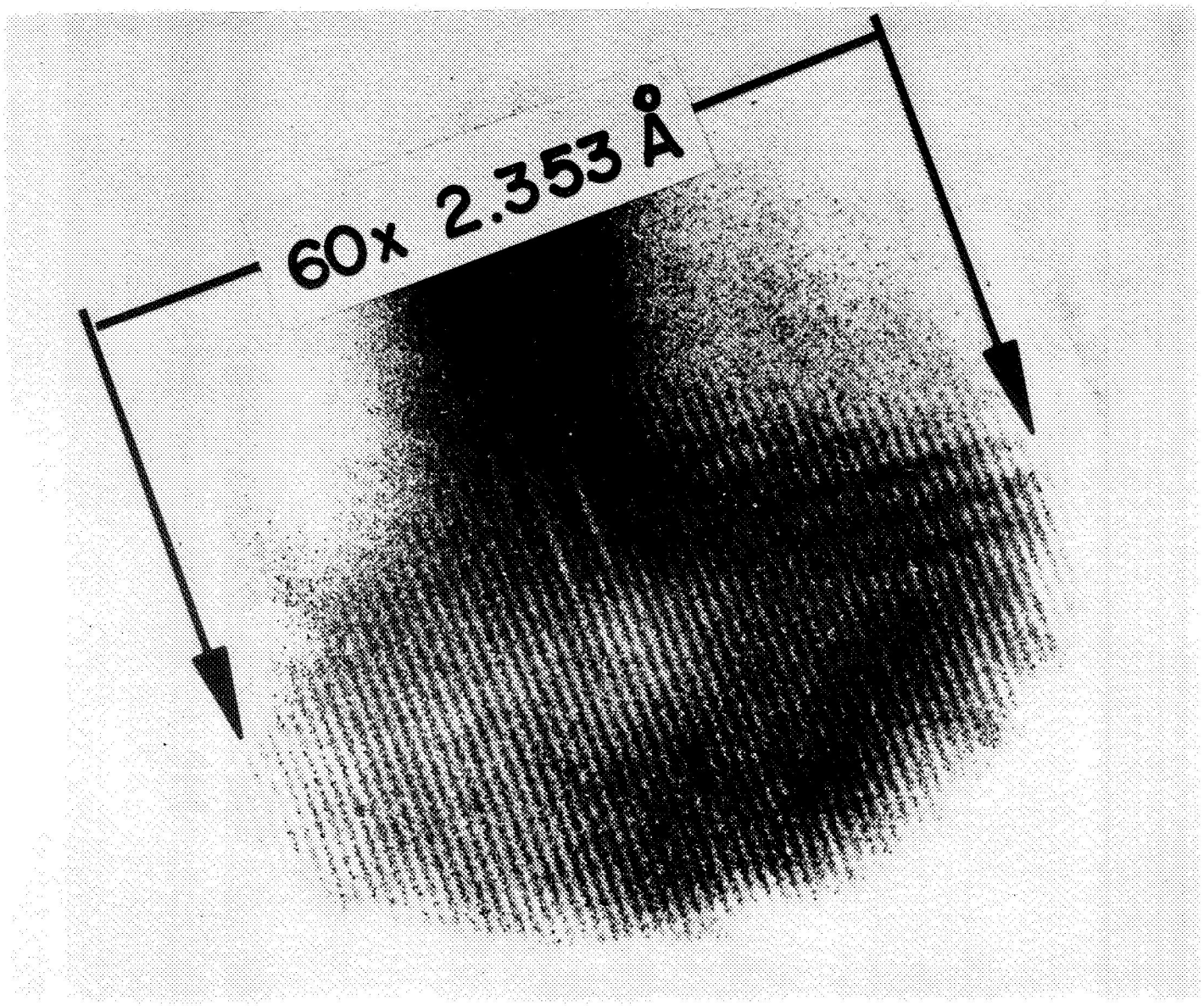

Figure 2.

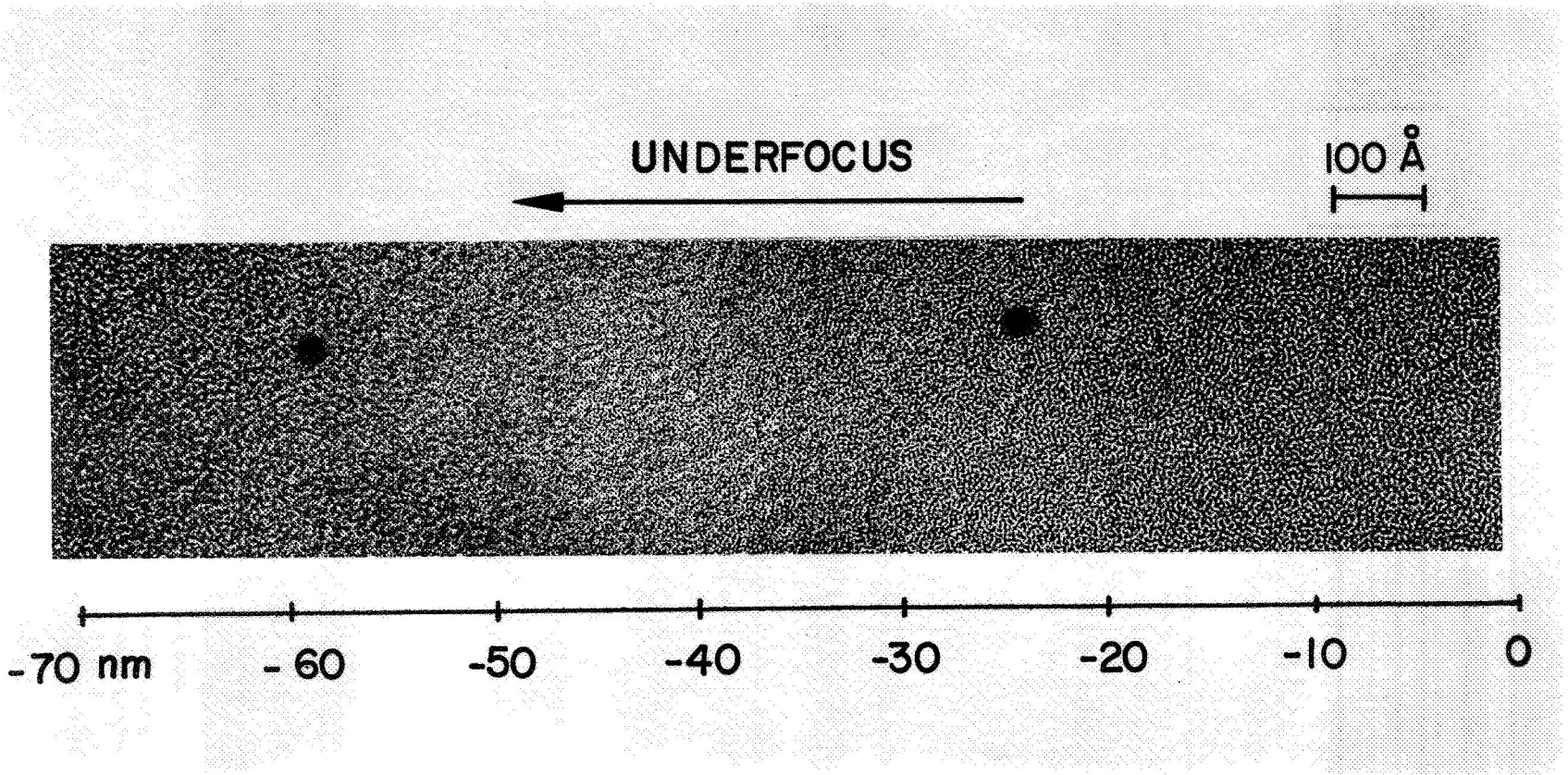

Figure 3.

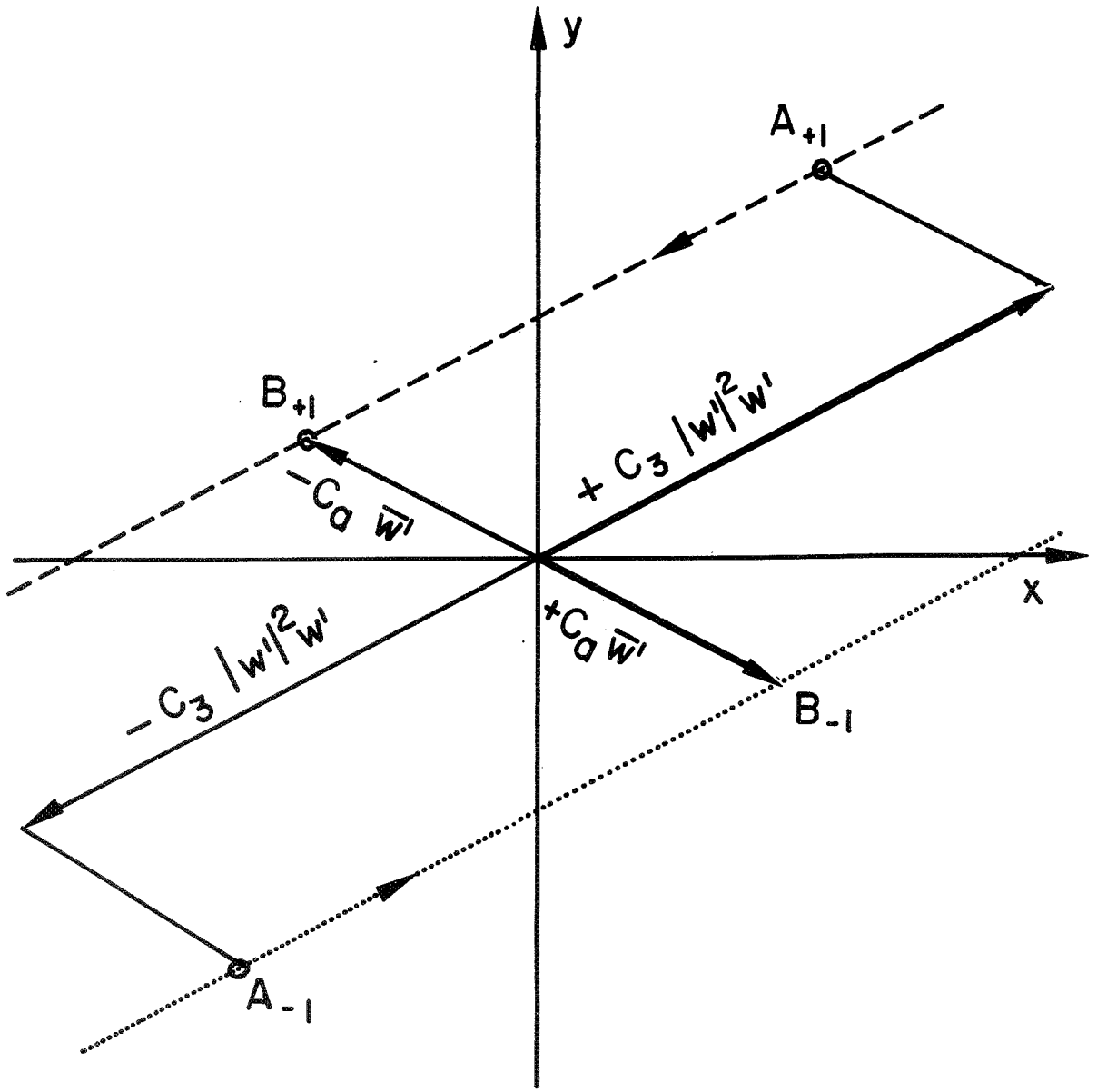

Figure 4.

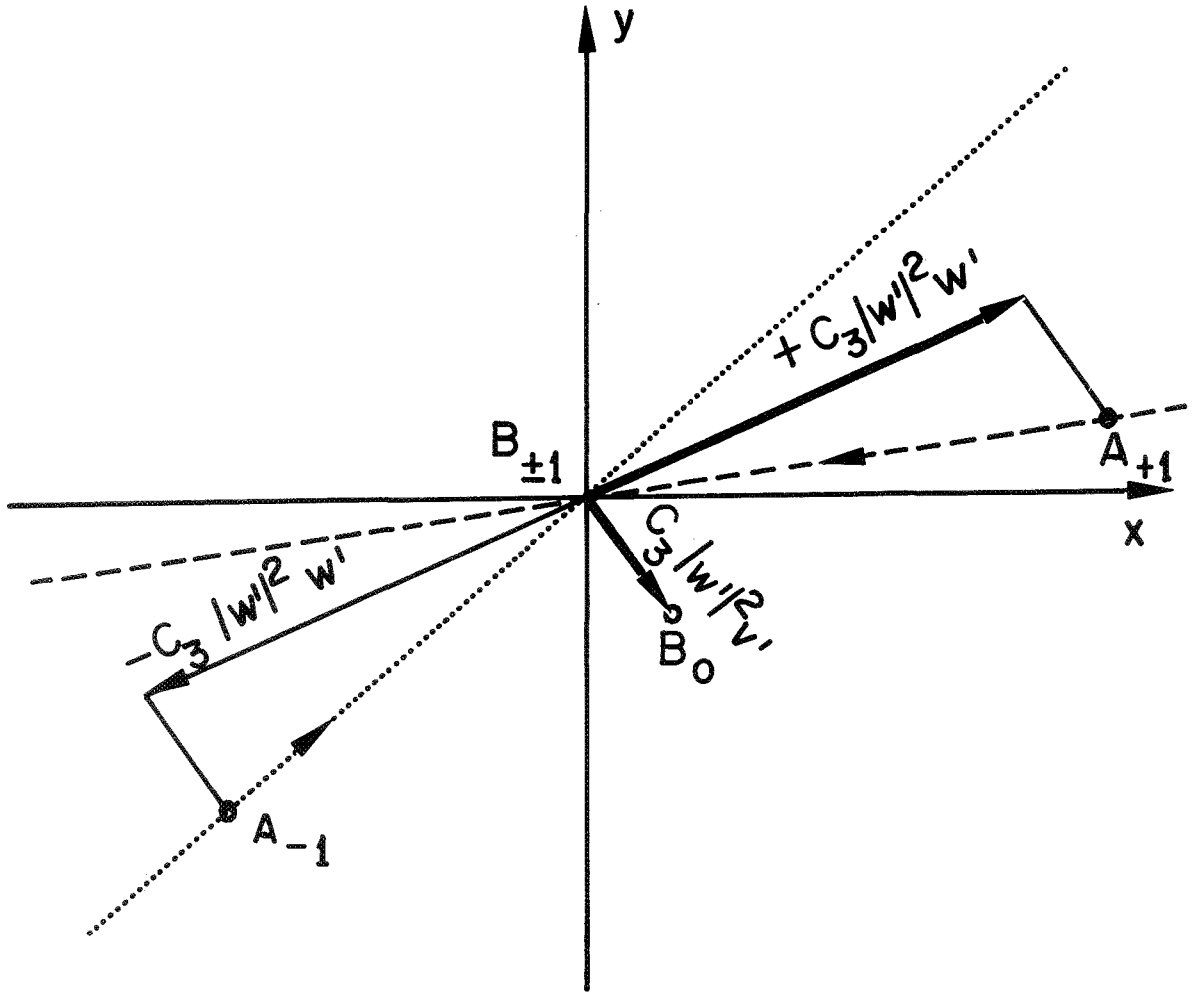

Figure 5.

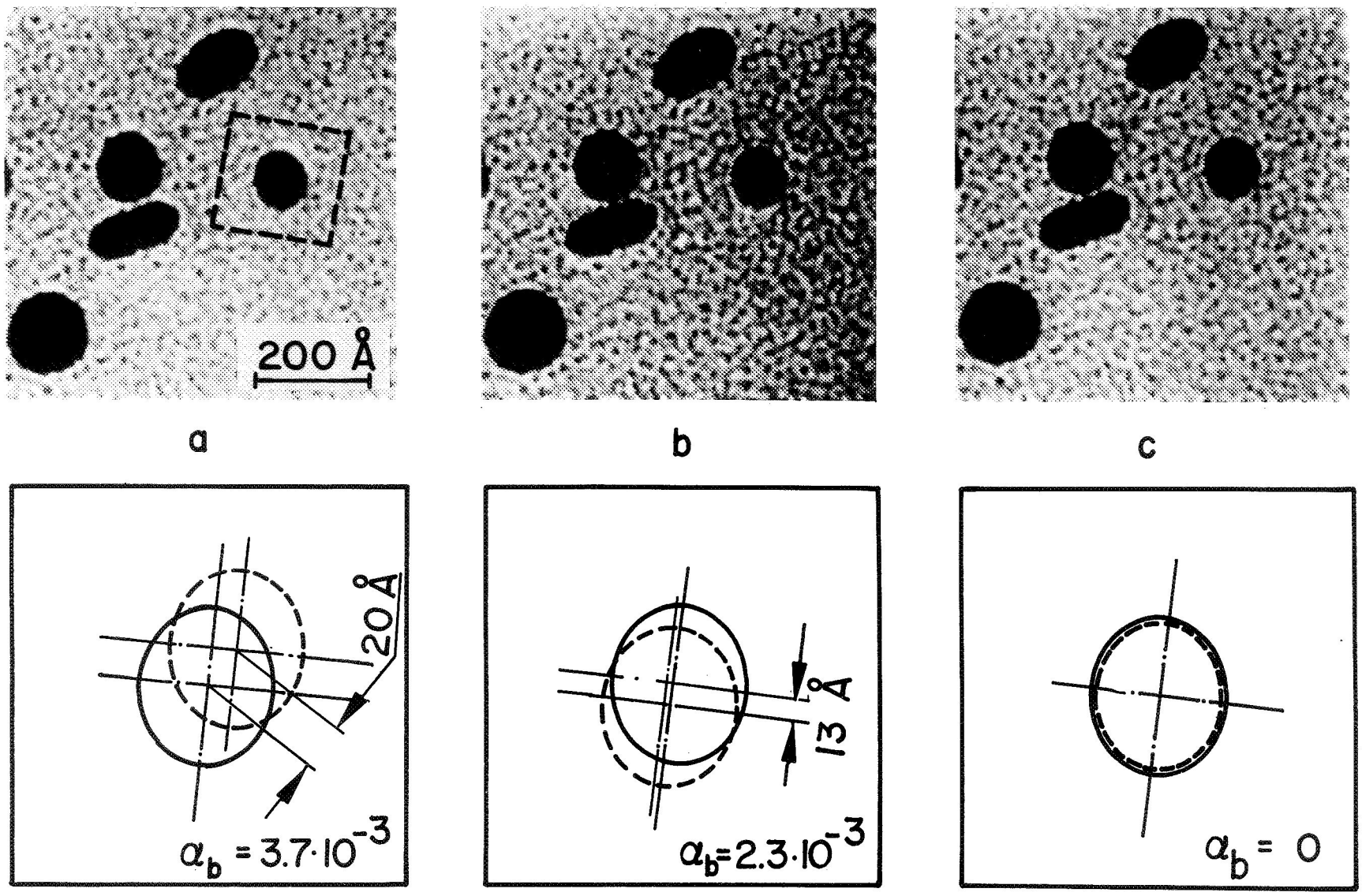
200 Å
a
b
c
20 Å
$\alpha_b = 3.7 \cdot 10^{-3}$
13 Å
$\alpha_b = 2.3 \cdot 10^{-3}$
$\alpha_b = 0$

Figure 6.

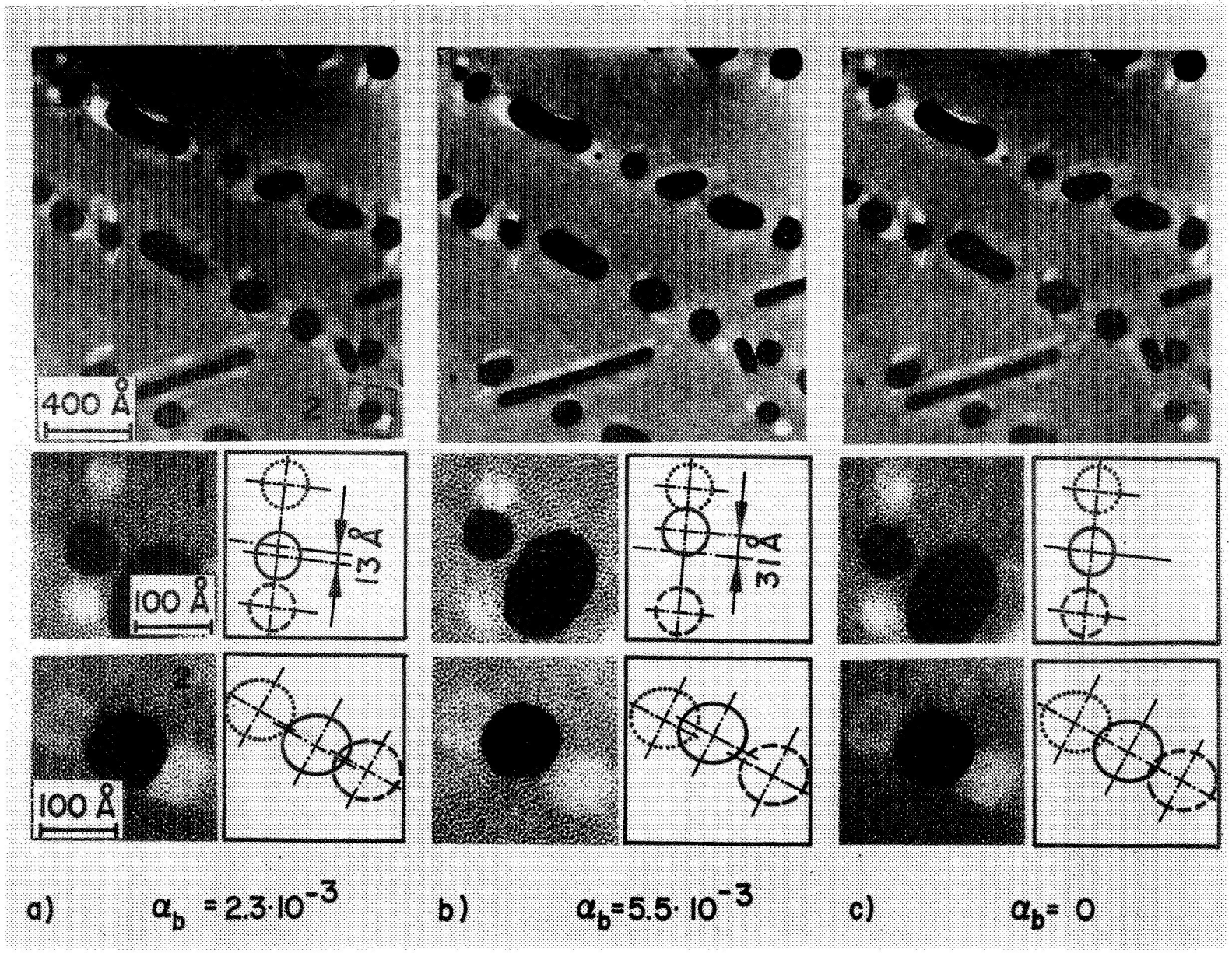
400 Å
1
2
100 Å
13 Å
31 Å
100 Å
a) $\alpha_b = 2.3 \cdot 10^{-3}$
b) $\alpha_b = 5.5 \cdot 10^{-3}$
c) $\alpha_b = 0$

Figure 7.

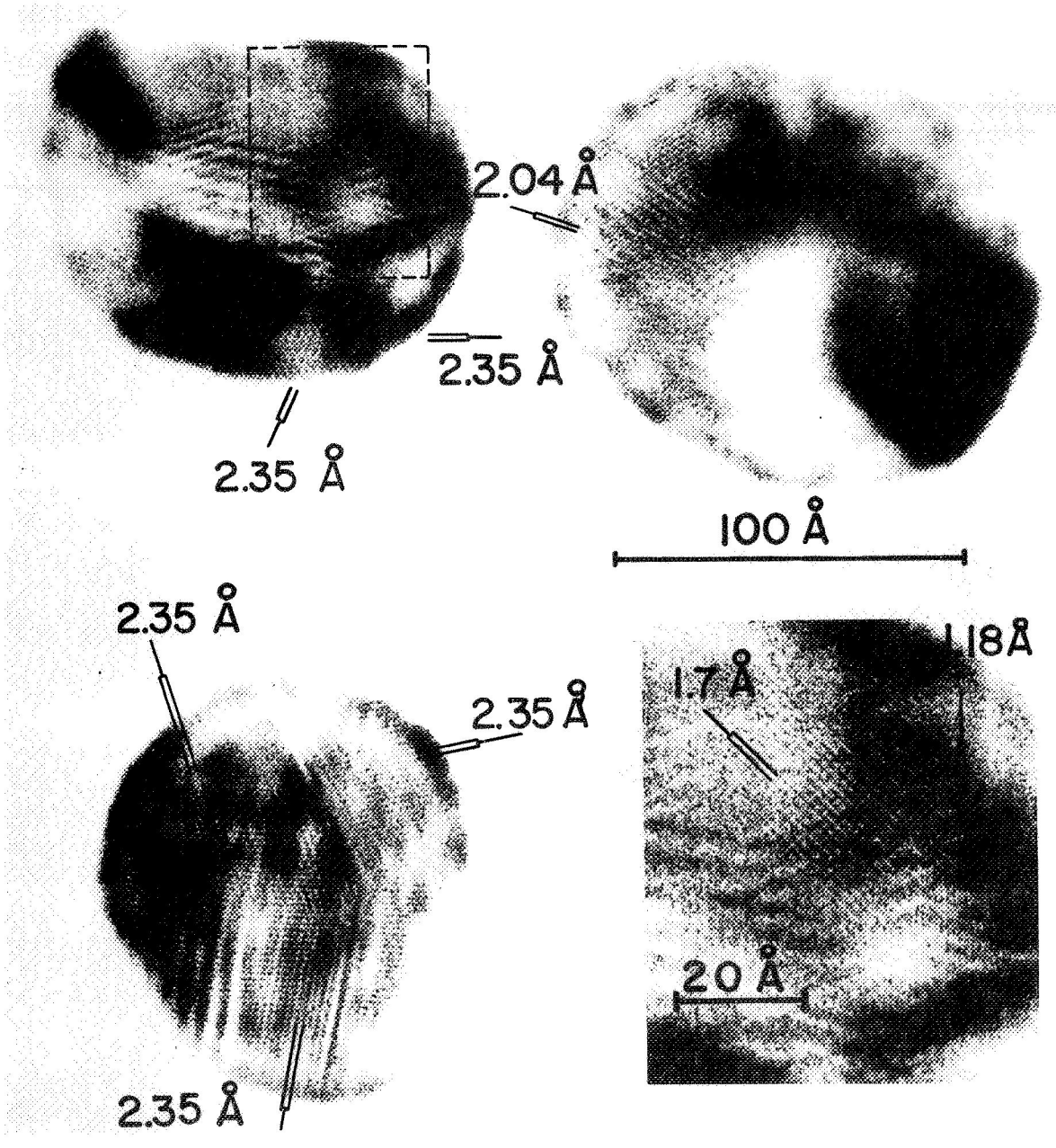

Figure 8.